ICRIE 2023 4th INTERNATIONAL CONFERENCE ON RECENT INNOVATIONS IN ENGINEERING

Proceedings of the 4th International Conference on Recent Innovation in Engineering
ICRIE 2023, University of Duhok, College of Engineering, 13th – 14th September 2023
(Special issue for Passer journal of basic and applied sciences)
Paper No. 19

Design a Robust Optimal Proportional-Integral-Derivative Controller for CE152 Magnetic Levitation System Using Bee Colony Algorithm

Hassan S. Al-Nahhal[1], Moayed Almobaied[2]
[1]Private researcher, Palestine
[2]Control Engineering and Smart Systems at Islamic University of Gaza, Palestine
halnahhal1@students.iugaza.edu.ps; malmobaied@iugaza.edu.ps

ABSTRACT

One of the most popular methods for giving feedback to the control loop in industrial control systems is the proportional-integral-derivative (PID) controller. The tuning of the PID controller, however, is currently being researched by engineers. In this research, a robust PID controller is proposed for the CE152 magnetic levitation system. Magnetic levitation, commonly referred to as maglev, is a technology that uses magnetic fields to levitate an object, such as a vehicle or train, above a track. By using magnetic forces to counteract gravitational and inertial forces, maglev systems can achieve frictionless movement and potentially higher speeds compared to conventional wheeled transportation. In this research, the robust PID controller is involved by computing all stabilized PID controller gains for the affine linear characteristic polynomial in the presence of uncertain parameters using the parameter space approach and the edge theorem. The results of the parameter space approach are ranges of PID gains (K_P, K_D, K_I). Here, the optimal PID gains were chosen by the Artificial Bee Colony optimization algorithm to get optimal performance for CE152 magnetic levitation. The research defines a specific performance index function that quantifies the system's time-domain step response criteria (small overshoot percentage with significant minimization of both settling and rising times). This index function is inversely proportional to the desired performance criteria, aiming to optimize the system's performance. MATLAB simulations are used to validate and demonstrate the efficiency of the proposed graphical method for enhancing stability in the maglev system.

KEYWORDS: robust control, Proportional-Integral-Derivative Controller (PID), Magnetic Levitation System, Bee Colony Algorithm, Edge theorem, Affine linear polynomial, uncertain parameters, Optimal control, PID gains.

1 INTRODUCTION

The Magnetic Levitation (Maglev) system is a technique that uses magnetic force manipulation to suspend an object in the air, effectively counteracting the force of gravity. In a maglev system, the object is levitated and held in a stable position without any physical contact with solid surfaces, thanks to the repulsive or attractive magnetic forces between magnets[4]. Maglev is a well-developed and rapidly expanding technology with diverse applications, and its common denominator is the absence of physical contact, which leads to minimal wear and friction. Maglev systems exploit the principles of magnetism to levitate objects or vehicles without the need for traditional mechanical contact with surfaces[5]. Maglev technology has a wide range of practical uses, and its ability to provide contactless support and precise control makes it suitable for various industrial applications, for example, high-speed train suspension,

superconductor rotor suspension of gyroscopes, rocket-guiding projects, magnetic bearings, and vibration isolation systems [6-11].

Maglev systems pose significant challenges due to their highly nonlinear behavior. The modelling and control research of the magnetic levitation system is crucial in both industry and academia. To address these challenges, two main approaches are commonly used for modeling: the linearized approach and the nonlinear approach. For linearized models, techniques such as PI, PID, fuzzy, and state feedback LQR are widely used as in[3, 12-14]. PID controller is one of the most common and straightforward control strategies used in various applications due to its simplicity and effectiveness. However, one of the greatest drawbacks of the PID controller is the tuning process for its gains (K_P, K_I, and K_D) [15]. Indeed, exact input-output feedback linearization and sliding mode control using Lyapunov functions are two promising methods for nonlinear control.[16-18].

Either of the aforementioned linear models methodologies consider the suggested controller's robustness in the presence of model uncertainties in the system. When dealing with uncertain systems, some parameters in the characteristic polynomial may be uncertain or subject to variations. These uncertain parameters can represent modelling errors, unknown disturbances, or variations in system parameters due to external factors. Depending on how these uncertain parameters are included in the polynomial coefficients, the polynomial family can be categorized into several types[19]:

1. Interval Coefficients: In this case, the uncertain parameters are represented as intervals, and the polynomial coefficients are bounded within these intervals. For example, if a parameter is denoted as 'a' and it is uncertain in the range [a_{min}, a_{max}], then the corresponding polynomial coefficient is considered to be within that interval.
2. Affine Linear Coefficients: The uncertain parameters are represented as affine linear functions of some variables. This means the polynomial coefficients are expressed as a linear combination of uncertain parameters and some variables. For instance, a coefficient 'b' might be defined as $b = p1x + p2y$, where '$p1$' and '$p2$' are uncertain parameters and 'x' and 'y' are some known variables.
3. Multilinear Coefficients: In this case, the polynomial coefficients are expressed as products of multiple uncertain parameters. For example, a coefficient 'c' might be defined as $c = p1 * p2 * p3$, where '$p1$', '$p2$', and '$p3$' are uncertain parameters.
4. Polynomial Coefficients: The uncertain parameters are included directly as coefficients of polynomial terms. For instance, a coefficient 'd' might be defined as $d = p1\ p2\text{^}2 + p3$, where '$p1$', '$p2$', and '$p3$' are uncertain parameters.

The classification into interval, affine linear, multilinear, and polynomial coefficients helps in characterizing the nature of uncertainty in the system's characteristic polynomial. The CE152 magnetic levitation system's resultant characteristic polynomial is of the affine linear type. This research shows how to use the parameter space approach to determine all stabilized PID controller parameters (KP, KI, KD) for magnetic levitation CE152 system with parametric variations with a characteristic polynomial of an affine linear. Furthermore, this research work presents the Artificial Bee Colony Algorithm developed effective PID gains for optimal performance (small overshoot percentage with significant minimization of both settling and rising times). The mathematical model of the CE152 magnetic levitation system is presented in Section II. The control design is introduced in Section III, which also lists the theoretical formulas and theoretical analyses of them. Section IV introduces the simulation results and explains the Artificial Bee Colony Algorithm and Section V presents the conclusion of the study.

2 MATHEMATICAL MODEL OF CE152 MAGNETIC LEVITATION SYSTEM

2.1 Introduction of Magnetic Levitation System

Figure 1 illustrates the Magnetic levitation CE152 model, which is comprised of a metal ball, coil, PC with Data Acquisition (DAQ) Card and power amplifier[20]. A steel ball (or any other magnetizable object) is levitated in the air through a delicate balance between the gravitational force and the magnetic

force created by an electromagnet. The control system's objective is to precisely control the magnetic force to counteract the gravitational force and keep the ball suspended at a desired height [2].

Figure 1: CE152 magnetic levitation[1]

2.2 Modelling of CE152 Magnetic Levitation System

The block diagram of CE152 is demonstrated in Figure 2, which consists of:

1. Digital-to-analogue converter K_{DA}.
2. Power amplifier (K_i, T_a).
3. Ball and coil (k_c, m_k).
4. Position sensor (k_x).
5. Analog-to-Digital converter (K_{AD}).

2.2.1 Digital-to-analogue converter subsystem

D/A converter can be characterized in terms of (1), which is represented by the Simulink block model, as shown in Figure 3.

$$u = k_{DA} u_{MU} + u_0 \qquad (1)$$

Where u is the model output voltage $[V]$, k_{DA} is the D/A converter gain $[V/MU]$, u_{MU} is the D/A converter input $[MU]$ and u_0 is the D/A converter offset $[V]$.

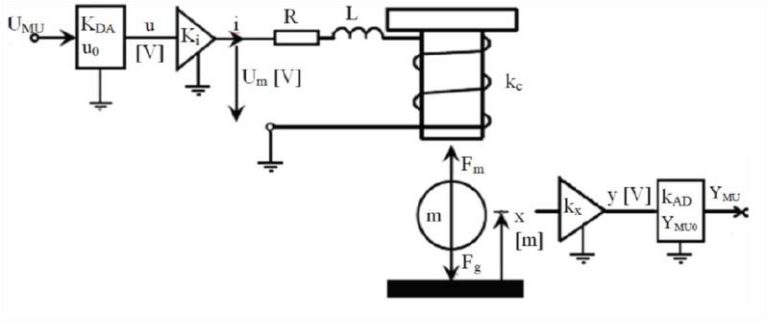

Figure 2: Schematic of the Magnetic levitation CE152 model[3]

Figure 3: . Digital-to-Analog converter subsystem

2.2.2 The power amplifier subsystem

Figure 4 demonstrates the internal structure of the power amplifier, which works as a constant current source with the feedback stabilization current. Equations (2) and (3) are obtained by applying the Kirchhoff's Voltage Law (KVL) to the power amplifier circuit.

$$U_m = L_c \frac{di}{dt} + (R_c + R_s)i \tag{2}$$

$$U_m = k_{am}(u - R_s i k_s) \tag{3}$$

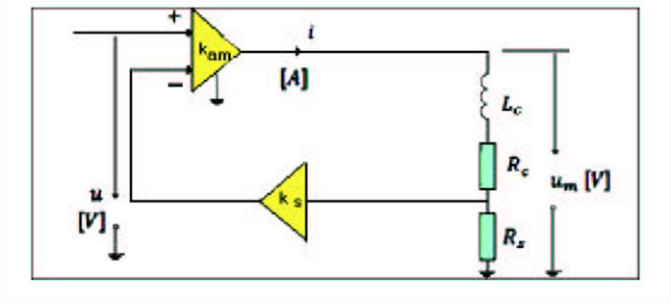

Figure 4*:* The power amplifie

The amplifier voltage u and the amplifier current i are considered the input voltage and the output current of the power amplifier, respectively. The power amplifier's transfer function is illustrated by solving (2) and (3) and applying the Laplace transform as follows:

$$\frac{I(s)}{U(s)} = \frac{k_{am}}{(L_c s + (R_c + R_s) + R_s k_s k_{am})} \tag{4}$$

$$\frac{I(s)}{U(s)} = \frac{\frac{k_{am}}{(R_c + R_s) + R_s k_s k_{am}}}{\left(\frac{L_c}{(R_c + R_s) + R_s k_s k_{am}} s + 1\right)} \tag{5}$$

Where,

$$k_i = \frac{k_{am}}{(R_c + R_s) + R_s k_s k_{am}} \tag{6}$$

$$T_a = \frac{L_c}{(R_c + R_s) + R_s k_s k_{am}} \tag{7}$$

The power amplifier's transfer function is represented by (8).

$$\frac{I(s)}{U(s)} = \frac{k_i}{(T_a s + 1)} \tag{8}$$

Where k_i and T_a are called the coil and amplifier gain and the coil and amplifier time constant, respectively. The inverse Laplace transform of the current is illustrated by (9).

$$i(t) = k_i(1 - e^{-\frac{t}{T_a}}) \tag{9}$$

2.2.3 Ball and Coil Subsystem

In a magnetic levitation system, the goal is to achieve levitation by creating a stable equilibrium where the forces on the levitated object (ball) are balanced, and there is no net force acting on it. At this point, the ball will float in the air, neither rising nor falling, effectively defying gravity, as shown in Figure 5.

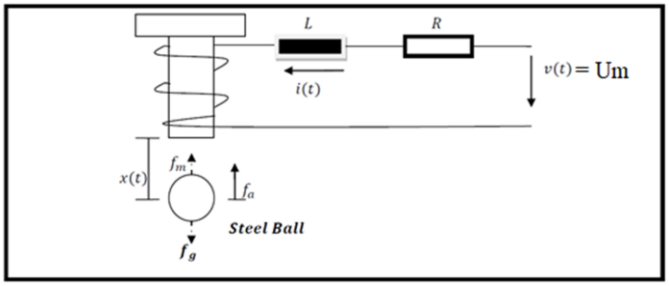

Figure 5: Magnetic Ball Levitation Subsystem[2]

Using Lagrange's equations, the model of the ball and coil for magnetic levitation can be described as follows[2].

$$\mathcal{L}(x, \dot{x}) = T - V = \frac{1}{2} m\dot{x}^2 - mgx \tag{10}$$

Where, T and V denote the ball's kinetic and potential energy, respectively. In the absence of any non-conservative external forces, Lagrange's equation for the magnetic levitation system is given by (11).

$$\frac{d}{dt}\frac{\partial \mathcal{L}}{\partial \dot{x}} - \frac{\partial \mathcal{L}}{\partial x} = m\ddot{x} + mg = 0 \tag{11}$$

Who forces are acting on the system, one of them is the force caused by air damping. F_d and the other is the force of the electromagnetic field F_m which can be obtained as follows.

Equations (12) demonstrate the energy in the coil which has N number of coil turns, l the coil length , μ is the permeability of the coil core, L is the inductance and A is the coil cross-section area .

$$W_m = \frac{1}{2} L i^2 \tag{12}$$

$$R = \frac{l}{\mu A} \tag{13}$$

$$L = \frac{N^2}{R} = \frac{\mu A N^2}{l} \quad (14)$$

$$W_m = \frac{\mu A N^2}{2l} i^2 \quad (15)$$

$$F_m = \frac{dW_m}{dl} = \frac{\mu A N^2}{2l^2} i^2 = k_c \frac{i^2}{(x - x_0)^2} \quad (16)$$

Where $k_c = \frac{\mu A N^2}{2}$ is the aggregated coil constant $[N/A]$, i is the coil current $[A]$, x is the distance $[m]$ and x_0 is the coil offset $[m]$.

The force caused by air damping F_d:

$$F_d = -k_{FV}\dot{x} \quad (17)$$

Where, k_{FV} is the damping constant $[N.s/m]$.
The two forces are appended as follows:

$$\frac{d}{dt}\frac{\partial \mathcal{L}}{\partial \dot{x}} - \frac{\partial \mathcal{L}}{\partial x} = F_m + F_d \quad (18)$$

From (11), (16), and (17):

$$m_k \ddot{x} + m_k g = k_c \frac{i^2}{(x - x_0)^2} - k_{FV}\dot{x} \quad (19)$$

Where. m_k is the ball mass $[kg]$ and g is the gravity acceleration $[m/s^2]$.
Equation (19) can be arranged as follows[2]:

$$m_k \ddot{x} = k_c \frac{i^2}{(x - x_0)^2} - m_k g - k_{FV}\dot{x} \quad (20)$$

2.2.4 Position sensor

The position of the ball can be measured by the position sensor which provides feedback into the system about the ball's position. Equation (21) represents the position sensor model.

$$y = k_x x + y_0 \quad (21)$$

Where; y is the model output voltage $[V]$, k_x is the position sensor gain $[V/m]$, x is the ball position $[m]$ and y_0 is position sensor offset $[m]$.

2.2.5 Analog-to-Digital converter subsystem

A/D converter can be demonstrated by (22).

$$y_{MU} = k_{AD} y + y_{MU0} \quad (22)$$

Where; y_{MU} is the A/D converter output $[V]$, k_{AD} is the D/A converter gain $[MU/V]$, y is the model output voltage $[V]$, and y_{MU0} is the A/D converter offset $[MU]$. Figure 6 represents the Simulink block diagram of the A/D converter and position sensor subsystem.

Figure 6: Simulink block diagram of A/D converter and position sensor subsystems

2.3 CE152 state space model

By supposing $\dot{x}_1 \triangleq x_2 \triangleq \dot{x}$, $i \triangleq x_3$, $A_1 = \frac{k_c}{m_k}$, $B_1 = \frac{k_{FV}}{m_k}$, $C_1 = k_{DA}k_i$, and $D_1 = k_{AD}k_x$. The state equations of the CE152 magnetic levitation system can be presented from (8), (20), and (2s) as shown in (23)[2].

$$\begin{bmatrix} \dot{x}_1 \\ \dot{x}_2 \\ \dot{x}_3 \\ y \end{bmatrix} = \begin{bmatrix} x_2 \\ A_1 \frac{x_3^2}{(x_1 - x_0)^2} - B_1 x_2 - g \\ \frac{1}{T_a} x_3 + \frac{C_1}{T_a} u \\ D_1 x_1 \end{bmatrix} \tag{23}$$

The state space model in the above equations gives evidence that the system is nonlinear. However, there are two famous methods for controlling the system: linear system control and nonlinear system control. The following section discusses the linearization process of the CE152 magnetic levitation system.

2.4 Linearization

The first-order differential equations of magnetic levitation are described in (23). By putting $\dot{x}_1 = \dot{x}_2 = \dot{x}_3 = 0$, the system's equilibrium points can be calculated. Which can be determined by solving the obtained system of nonlinear equations. Suppose that the equilibrium point at (x_{10}, x_{20} , x_{30}) then, $x_{20} = 0$ and $x_{30} = (x_{10} - x_0)\sqrt{\frac{g}{A_1}}$ [2]. A first-order approximation of the Taylor series expansion near the unstable equilibrium point (x_{10}, x_{20} , x_{30}) will be used to linearize equation (23) [21, 22]. The following nonlinear differential equations can be used to represent the dynamic behavior of the magnetic levitation system in equation (23).

$$\begin{aligned} f_1(x_1, x_2, x_3, u) &= x_2 \\ f_2(x_1, x_2, x_3, u) &= A_1 \frac{x_3^2}{(x_1 - x_0)^2} - B_1 x_2 - g \\ f_3(x_1, x_2, x_3, u) &= -\frac{1}{T_a} x_3 + \frac{C_1}{T_a} u \end{aligned} \tag{24}$$

First, the dynamic behavior (24) is assumed to be acting at its equilibrium point (x_{10}, x_{20} , x_{30}). If the system (24) is now perturbed, it will keep acting in the orientation of $x_1 = x_{10} + \delta x_1$, $x_2 = x_{20} + \delta x_2$, $x_3 = x_{30} + \delta x_3$ and $u = u_0 + \delta u$, where δx_1, δx_2, δx_3 and δu are illustrated as the impacts of the perturbation in the dynamic system.

A Taylor series expansion can be applied to (24) around the equilibrium point (x_{10}, x_{20} , x_{30}), leading to the following equation:

$$\begin{aligned} f(x_1, x_2, x_3, u) = &\frac{\partial}{\partial x_1} f(x_{10}, x_{20}, x_{30}, u_0) \frac{(x_1 - x_{10})}{1!} + \frac{\partial}{\partial x_2} f(x_{10}, x_{20}, x_{30}, u_0) \frac{(x_2 - x_{20})}{1!} \\ &+ \frac{\partial}{\partial x_3} f(x_{10}, x_{20}, x_{30}, u_0) \frac{(x_3 - x_{30})}{1!} + \frac{\partial}{\partial u} f(x_{10}, x_{20}, x_{30}, u_0) \frac{(u - u_0)}{1!} + H.O.T \end{aligned} \tag{25}$$

By neglecting the H.O.T and considering partial derivatives at the equilibrium point (x_{10}, x_{20} , x_{30} , u_0), the Taylor expansion (25) can be reduced if the disturbances are small enough. Results that will be attained include:

$$f_2(x_1, x_2, x_3, u) = \frac{-A_1 x_{30}^2}{(x_1 - x_0)^3}\delta x_1 - B_1 \delta x_2 + \frac{A\_1\, x_{30}}{(x_1 - x_0)^2}\delta x_3 \tag{26}$$

$$f_3(x_1, x_2, x_3, u) = -\frac{1}{T_a}\delta x_3 + \frac{C_1}{T_a}\delta u \tag{27}$$

Equations (26) and (27) are represented the linear state equations of the magnetic levitation system. As a result, the state space model can be arranged as the following.

$$\begin{bmatrix}\dot{x}_1\\ \dot{x}_2\\ \dot{x}_3\end{bmatrix} = \begin{bmatrix} 0 & 1 & 0 \\ \frac{-A_1 x_{30}^2}{(x_1 - x_0)^3} & -B_1 & \frac{A_1 x_{30}}{(x_1 - x_0)^2} \\ 0 & 0 & -\frac{1}{T_a}\end{bmatrix}\begin{bmatrix}x_1\\ x_2\\ x_3\end{bmatrix} + \begin{bmatrix}0\\ 0\\ \frac{C_1}{T_a}\end{bmatrix} u \tag{28}$$

$$[y] = [D_1 \quad 0 \quad 0]\begin{bmatrix}x_1\\ x_2\\ x_3\end{bmatrix}$$

The CE152 model parameters used in modelling the system are described in Table 1.

The state space model and transfer function of the system at $x_{10} = 0.0032$,$x_{20} = 0$ and $x_{30} = 0.5723$ can be described as the following.

$$\begin{bmatrix}\dot{x}_1\\ \dot{x}_2\\ \dot{x}_3\end{bmatrix} = \begin{bmatrix} 0 & 1 & 0 \\ 395.5 & -2.4 & 36 \\ 0 & 0.1988 & -5.3492e4\end{bmatrix}\begin{bmatrix}x_1\\ x_2\\ x_3\end{bmatrix} + \begin{bmatrix}0\\ 0\\ 1.5873e5\end{bmatrix} u \tag{29}$$

$$[y] = [159.4921 \quad 0 \quad 0]\begin{bmatrix}x_1\\ x_2\\ x_3\end{bmatrix}$$

$$G(s) = \frac{9.06e08}{s^3 + 5.349e04\, s^2 + 1.234e05\, s - 2.116e08} \tag{30}$$

The location of the open loop transfer function poles at $62, -64$, and $-5.3492e4$. There is one pole on the right half plane (RHP), which causes the system to be unstable. As a result, it is required to add a controller to stabilize the system. However, the purpose of the Maglev's control design is to develop a controller that levitates the steel ball from its starting location and forces it to follow a special position trajectory. This will be discussed in the following section.

Table 1: CE152 model parameters[1]

Parameter	Symbol	Value
ball mass [kg]	mk	0.0084
viscose friction[unitless]	KFv	0.02
ball diameter [m]	Dk	12.7e-3
gravity acceleration constant [$m.s^{-2}$]	g	9.81
maximum DA converter output voltage[unitless]	U_DAm	5
coil resistance [Ohm]	Rc	3.5
coil inductance [H]	Lc	30e-3
current sensor resistance [Ohm]	R_s	0.25

current sensor gain [unitless]	k_s	13.33
power amplifier gain [unitless]	K_am	100
maximum power amplifier output current[A]	I_am	1.2
amplifier time constant [s]	T_a	1.8694e-05
amplifier gain [A/V]	k_i	0.2967
D/A converter gain[unitless]	k_DA	10
A/D converter gain[unitless]	k_AD	0.2
position sensor constant[unitless]	k_x	797.4603
aggregated coil constant[N/V]	k_f	0.606e-6
coil constant[unitless]	k_c	6.8823e-06
coil limit bias [m]	x_0	8.26e-3

3 CONTROL DESIGN

In a magnetic levitation (maglev) system, there are two main subsystems: the electrical subsystem **(**Current Loop**)** and the mechanical subsystem**.** The interaction between these two components allows for indirect control of the position of the levitated ball. A proportional-integral-derivative (PID) controller will be designed in this study with the presence of uncertain parameters in the system. Using a PID controller, the mechanical subsystem can track the target position with the elimination of the error and a sensible velocity. The classical PID control method does not explicitly account for parametric uncertainty, and its performance may degrade or become unstable in the presence of such uncertainties. Robust control, on the other hand, is a branch of control theory that focuses on designing controllers that can handle parametric uncertainties and external disturbances while maintaining desired performance and stability.

In this study, both m_k and K_{Fv} were chosen as uncertain parameters such that $m_k \in [0.008, 0.0088]$ and $K_{Fv} \in [0.015, 0.025]$. As a result, the following will be the transfer function:

$$G(s, m_k, K_{Fv}) = \frac{4.5e7}{5.92m_k s^3 + (5.92K_{Fv} + 3.17m_k e5)s^2 + (3.17K_{Fv} e5 - 197)s - 1.05e7} \quad (31)$$

The characteristic polynomial is:

$$P(s, m_k, K_{Fv}) = 5.92m_k s^3 + (5.92K_{Fv} + 3.17m_k e5)s^2 + (3.17K_{Fv} e5 - 197)s - 1.05e7 \quad (32)$$

The unknown parameters in the robust theory of control are represented by the symbol q, e.g., $q_1 \triangleq m_k$, $q_2 \triangleq K_{Fv}$. As a result, the characteristic equation can be rewritten as:

$$P(s, q_1, q_2) = 5.92q_1 s^3 + (5.92q_2 + 3.17q_1 e5)s^2 + (3.17q_2\, e5 - 197)s - 1.05e7 \quad (33)$$

The aforementioned polynomial family belongs to the affine polynomial class, in which the uncertain parameters q_1 and q_2 are linearly entered into the polynomial coefficients.

3.1 Stability test for the affine linear polynomial

In an l-dimensional box Q, the parameters q_i alter.

$$q_i \in [q_i^-, q_i^+], i = 1,2, \dots, l \quad (34)$$

The parameter box Q comprises the two uncertain variables: q_1 and q_2, is shown in Figure 7.

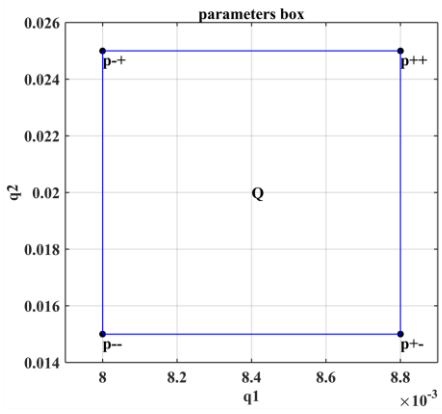

Figure 7: Parameter box

In the context of uncertain polynomial systems, the vertex polynomials are obtained by considering the extreme values of the uncertain parameters at the vertices of the parameter box Q. Each vertex of the parameter box represents a specific combination of the uncertain parameters, and evaluating the polynomial with these extreme values provides the corresponding vertex polynomial. However, when dealing with the affine-linear polynomial family and its stability analysis, checking the stability of the vertex polynomials alone is insufficient to assess the stability of the entire uncertain system. The reason lies in the nonlinearity introduced by the uncertain parameters in the polynomial. In general, the parameter space can be represented as a hypercube or parameter box in l -dimensional space. Each vertex of this hypercube represents a specific combination of the uncertain parameters, and there are 2^l vertices in total. The edge polynomials are a set of polynomials derived from the uncertain polynomial family, where one of the uncertain parameters varies between its maximum and minimum values, while the remaining $l-1$ parameters are held constant at specific values. By considering all possible combinations of fixing $l-1$ parameters and varying the remaining one, we obtain $l2^{l-1}$ edge polynomials [19]. The robust stability of an affine linear polynomial family and its edge polynomials are equivalent. If the family is robustly stable, all edge polynomials are robustly stable, and conversely, if all edge polynomials are robustly stable, the entire family is robustly stable. This relationship simplifies the analysis and design of robustly stable controllers for uncertain systems represented by affine linear polynomial families. [23]. In the case of $l = 2$ and any ω, the value set of the polynomial family can be visualized as shown in figure 8. $P^1(s)$, $P^2(s)$, $P^3(s)$and $P^4(s)$ represent the vertex polynomials. The edge polynomials can be defined as shown in Table 2.

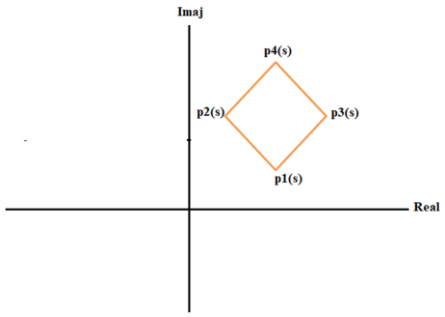

Figure 8: The value set of the polynomial with specific ω and $l = 2$

Table 2: The edge polynomials when $\boldsymbol{l = 2}$

The edge polynomials	
$\boldsymbol{p^{(12)} = (1-\lambda)P^1(s) + \lambda P^2(s)}$	$\boldsymbol{\lambda \in [0,1]}$
$\boldsymbol{p^{(13)} = (1-\lambda)P^1(s) + \lambda P^3(s)}$	$\boldsymbol{\lambda \in [0,1]}$
$\boldsymbol{p^{(42)} = (1-\lambda)P^4(s) + \lambda P^2(s)}$	$\boldsymbol{\lambda \in [0,1]}$
$\boldsymbol{p^{(43)} = (1-\lambda)P^4(s) + \lambda P^3(s)}$	$\boldsymbol{\lambda \in [0,1]}$

By supposing the edge polynomial family as follows:

$$p^{(ab)} = (1-\lambda)P^a(s) + \lambda P^b(s) \qquad \lambda \in [0,1] \tag{35}$$

Where, $P^a(s) = P_{a0} + P_{a1}s + P_{a2}s^2 + \cdots + P_{an}s^n \quad P_{an} > 0$ and $P^b(s) = P_{b0} + P_{b1}s + P_{b2}s^2 + \cdots + P_{bn}s^n \quad P_{bn} > 0$. The Bialas theorem is used to guarantee a stability for edge polynomials families. Such that $p^{(ab)}$ is robust and stable if and only if the $P^a(s)$ is stable , $P^b(0) = P_{b0} > 0$ and the Hurwitz matrices of $(H^a_{n-1})^{-1}H^b_{n-1}$ has no nonpositive real eigenvalues[19].

The controller design should be applied to four vertices of the polytypic system using the Edge Theorem, and then the stability of each edge polynomial must be verified using the Bialas Theorem. Using the parameter space approach, all PID controller coefficients can be obtained so that the vertices of the polytypic system and the edge polynomials are stable. All these coefficients guarantee the stability of the desired closed-loop system[24].

3.2 Robust Stabilization PID Controller Design

There are several established methods for tuning PID controllers in the literature, such as Ziegler Nichols and Nyquist approaches. Traditional techniques, on the other hand, will supply designers with only one set of PID parameter values (K_P ,K_I , and K_D). A parameter space approach, on the other hand, is a graphical strategy for locating all stability zones of PID parameters and is considered a strong tool for robust stabilization challenges[15].

The open loop uncertain transfer function is shown in (36).

$$G(s, q_1, q_2) = \frac{4.5e7}{5.92q_1s^3 + (5.92q_2 + 3.17q_1e5)s^2 + (3.17q_2\, e5 - 197)s - 1.05e7} \tag{36}$$

The conventional PID controller has the following transfer function:

$$G_{PID}(s) = \frac{K_Ds^2 + K_Ps + K_I}{s} \tag{37}$$

The closed-loop PID controller for the uncertain magnetic levitation system is shown in Figure 9.

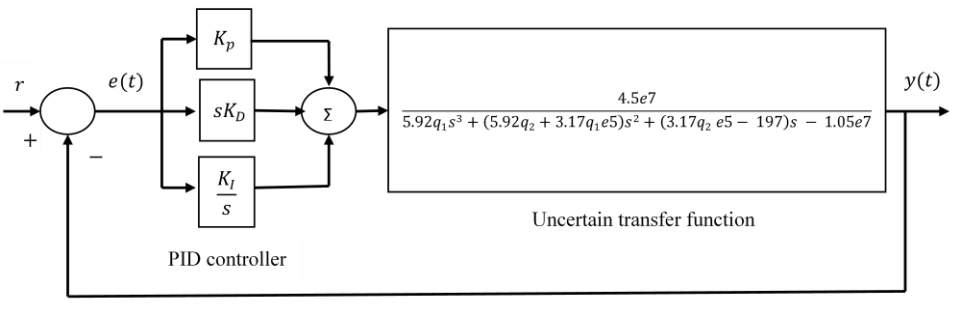

Figure 7: The closed loop PID controller for the uncertain magnetic levitation system model.

Suppose the open loop transfer function $G(s) = \frac{N(S)}{D(S)}$, then the close loop transfer function after adding the PID controller will be as shown in (38).

$$G(s)_{close\ loop} = \frac{G(S)_{PID}G(S,q_1,q_2)}{1+G(S)_{PID}G(S,q_1,q_2)} = \frac{\frac{K_DS^2+K_PS+K_I}{S}\frac{N(S)}{D(S)}}{1+\frac{K_DS^2+K_PS+K_I}{S}\frac{N(S)}{D(S)}} = \frac{(K_DS^2+K_PS+K_I)N(S)}{SD(S)+(K_DS^2+K_PS+K_I)N(S)} \quad (38)$$

The closed loop characteristic polynomial can be obtained from (36) and (38) as follows:

$$P(s,q_1,q_2,K_D,K_P,K_I) = 5.92q_1s^4 + (5.92q_2 + 3.17q_1e5)s^3 + (3.17q_2\ e5 + K_D4.5e7 - 197)s^2 + (K_P4.5e7 - 1.05e7)s + K_I4.5e7 \quad (39)$$

Table 3 demonstrates the vertex polynomials for the closed loop characteristic polynomial.

Table 3: The vertex polynomials for the affine linear polynomial

		Vertex polynomial
$\boldsymbol{P(s,q_1^-,q_2^-)}$	$p^{(1)}$	$= 0.04736s^4 + 2536.089s^3 + (4558 + K_D4.5e7)s^2 + (K_P4.5e7 - 1.05e7)s + K_I4.5e7$
$\boldsymbol{P(s,q_1^-,q_2^+)}$	$p^{(2)}$	$= 0.04736s^4 + 2536.148s^3 + (7728 + K_D4.5e7)s^2 + (K_P4.5e7 - 1.05e7)s + K_I4.5e7$
$\boldsymbol{P(s,q_1^+,q_2^-)}$	$p^{(3)}$	$0.0521s^4 + 2789.689s^3 + (4558 + K_D4.5e7)s^2 + (K_P4.5e7 - 1.05e7)s + K_I4.5e7$
$\boldsymbol{P(s,q_1^+,q_2^+)}$	$p^{(4)}$	$0.0521s^4 + 2789.748s^3 + (7728 + K_D4.5e7)s^2 + (K_P4.5e7 - 1.05e7)s + K_I4.5e7$

Equations (40) and (41), respectively, represent the real and the imaginary parts of the characteristic polynomial$P^{--}(s,K_D,K_P,K_I)$.

$$P_{Real}^{--} = 0.04736\omega^4 - (4558 + K_D4.5e7)\omega^2 + K_I4.5e7 \quad (40)$$

$$P_{Img}^{--} = -2536.089\omega^3 + (K_P4.5e7 - 1.05e7)\omega \quad (41)$$

Equations (40) and (41) can be rewritten in a matrix form as shown in (42).

$$\begin{bmatrix} 4.5e7 & -4.5e7\omega^2 \\ 0 & 0 \end{bmatrix}\begin{bmatrix} K_I \\ K_D \end{bmatrix} + \begin{bmatrix} -0.04736\omega^4 - 4558\omega^2 \\ -2536.089\omega^3 + (K_P4.5e7 - 1.05e7)\omega \end{bmatrix} = 0 \quad (42)$$

The parameter space method is an effective choice when dealing with systems with a small number of uncertain parameters, typically two or fewer. In such cases, exploring the parameter space becomes manageable, and the stability analysis can be performed efficiently. When there are more than two uncertain parameters, exhaustive exploration of the entire parameter space becomes computationally intensive, and alternative methods are often employed to assess stability regions. One such approach, as you mentioned, is to fix all parameters except the two parameters of interest and analyze the stability of the system for different combinations of these two parameters. Regarding PID controllers, there is a special scenario where it is sufficient to analyze the stabilization areas (regions of stability) for a fixed value of the proportional gain (K_P). In this case, fixing K_P and exploring the stability regions in the two-dimensional space of the remaining gains (K_D and K_I) can provide valuable insights into the system's stability. If the stabilization areas for a fixed K_P value is polygonal in geometry, which means that the regions of stability form polygons

in the (K_D, K_I) parameter space. This polygonal shape implies that the system's stability is influenced in a specific and predictable manner by the variations of K_D and K_I. The vertices of these stability polygons correspond to the edges of the parameter space where the system transitions between stability and instability[19]. Equation (42) is definitely of the pattern $Ax + b = 0$, and in order to obtain a solution, the determinant of matrix A should not equal zero. In this scenario, the determinant of the matrix A is:

$$Det(A) = \begin{vmatrix} 4.5e7 & -4.5e7\omega^2 \\ 0 & 0 \end{vmatrix} \quad (43)$$

The above determinant vanishes for any ω. consequently, the solution for K_I and K_D in (40) and (41) look to be either parallel lines or identical in the parametric surface, rather than a point. To ensure that the two lines are equal, the parameter KP's value must be supplied within the following range.

$$\frac{0}{4.5e7} = \frac{0}{-4.5e7\omega^2} = \frac{-2536.089\omega^3 + (K_P 4.5e7 - 1.05e7)\omega}{-0.04736\omega^4 - 4558\omega^2} \quad (44)$$

Then,

$$\omega^2 = \frac{(-1.05e7 + K_P 4.5e7)}{2536.089} \quad (45)$$

Because the frequency has to be positive, the value of K_P is chosen such that $(-1.05e7 + K_P 4.5e7) \geq 0$. As a result, the constraint $K_P \geq \frac{7}{30}$ guarantees that the lines in (40) and (41) are equivalent. When $K_P = 1$ is used, the value of ω is equal to 116.635, as shown in (45) or Figure 10(a). which graphically displays the link between K_P and w. The following results can be obtained by substituting the value of K_P in (40) and (41):

$$P^{--}_{Real} = 0.04736\omega^4 - (4558 + K_D 4.5e7)\omega^2 + K_I 4.5e7 \quad (46)$$

$$P^{--}_{Img} = -2536.089\omega^3 + 3.45e7\omega \quad (47)$$

Figure 11(a) demonstrates the stability areas of both K_I and K_D for P^{--}, where:

1. Real root boundary (RRB) at $\omega = 0$ is $K_I = 0$.
2. Infinity root boundary (IRB) at $\omega = \infty$ does not exist.
3. Complex root boundary (CRB) at $\omega = 116.635$.

$$K_I = 1.183 + 1.36e4K_D \quad (48)$$

The curves in Figure 11(a) split the plot into four distinct zones. If one of these regions has a stable polynomial, the rest of the territory must likewise have stable polynomials, according to the Boundary Crossing Theorem. The rest of the region must be containing unstable polynomials if one of these regions contains an unstable polynomial. As a result, by picking one polynomial for each region and testing its stability, the collection of stability zones may be adequately defined [25]. When this approach is applied to the graph in Figure 11(a), only one stable zone is visible. However, the numbers (0,1,2,3) in the graph represent the number of unstable poles in The zone. The preceding approaches should be applied to the P^{-+} , P^{+-} , and P^{++} vertex polynomials family. Figure 10(b), figure 10(c), and figure 10(d) demonstrate the connection between K_P and ω for both P^{-+}, P^{-+} , P^{+-} , and P^{++} ,respectively.

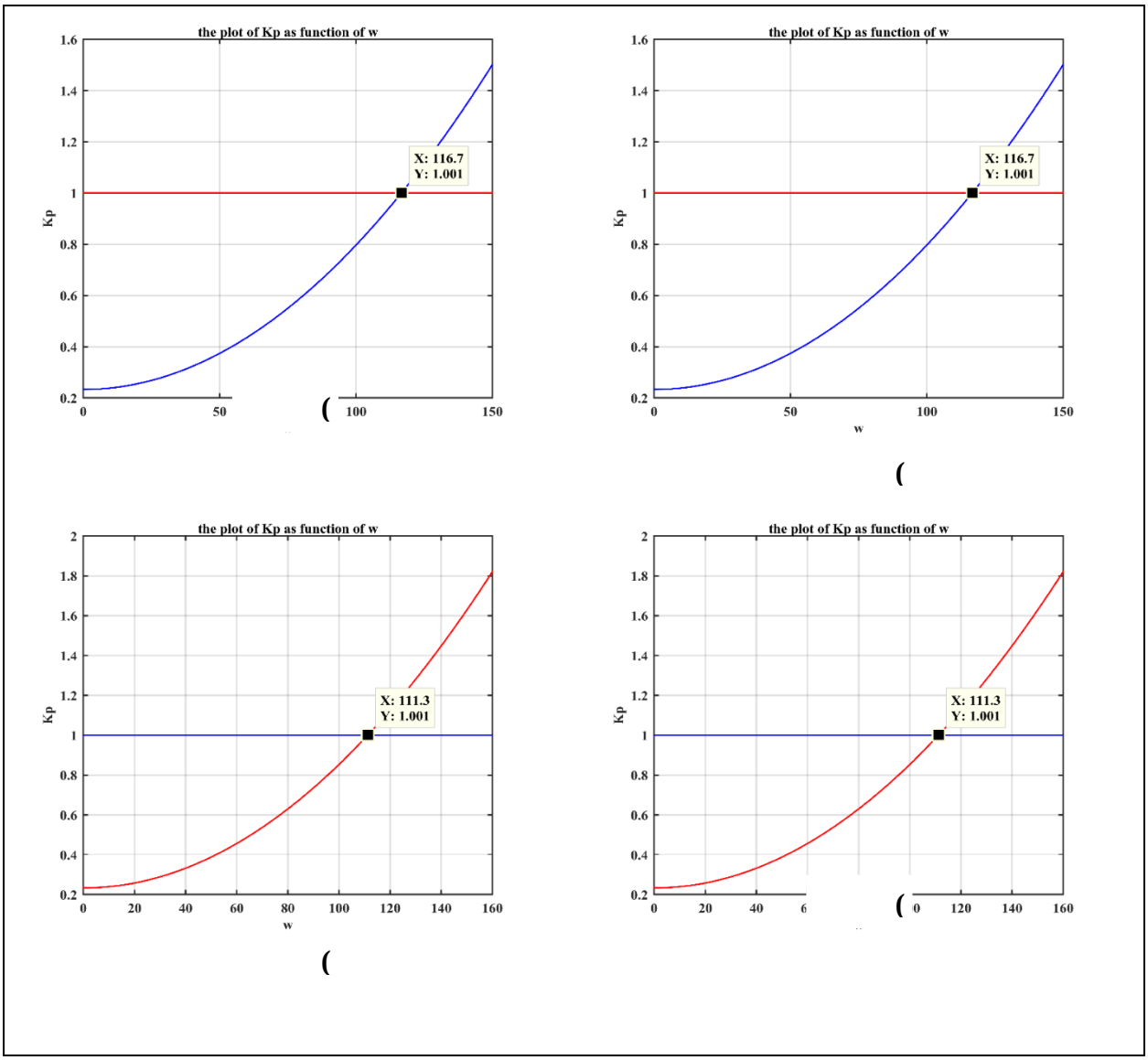

Figure 10: (a): Kp as function of ω for P^{--}, (b): Kp as function of ω for P^{-+},(c): Kp as function of ω for P^{+-},and (d) Kp as function of ω for P^{++}

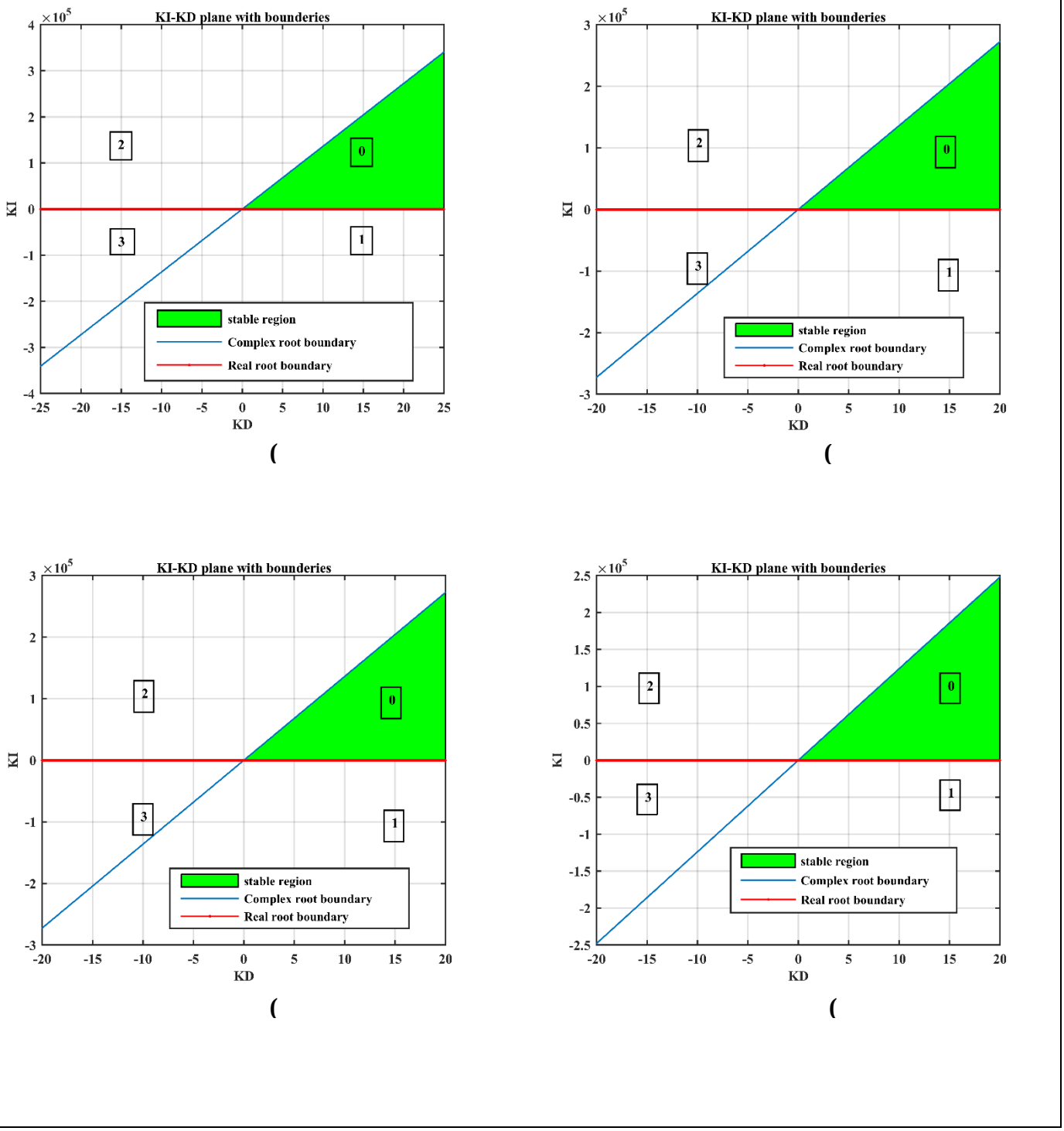

Figure 8: (a): K_I and K_D Plane for P^{--},(b): K_I and K_D Plane for P^{+-}, (c): K_I and K_D Plane for P^{-+}, and (d): K_I and K_D Plane for P^{++}

Figures 11 (b), (c), and (d) show how the RRB and CRB lines for P^{-+}, $P^{+-}$and P^{++} respectively, divide the "KI KD" plane into four new sections. As a result, in the same way as in the previous situation, the stable area of P^{-+}, $P^{+-}$and P^{++} can be recognized. By comparing the stability zones for P^{--}, P^{-+}, $P^{+-}$and P^{++} in figure 12, the stability region for P^{++} can be recognized as it is a subset of the P^{--}, P^{-+}, P^{+-}. As a result, the stability region of P^{++} guarantees the stability area for the original polynomial family. As a result, The range of $K_D \geq 8.7074e-05$ and the $0 < K_I < \frac{5.57e11 * K_D + 4.85e7}{4.5e7}$.

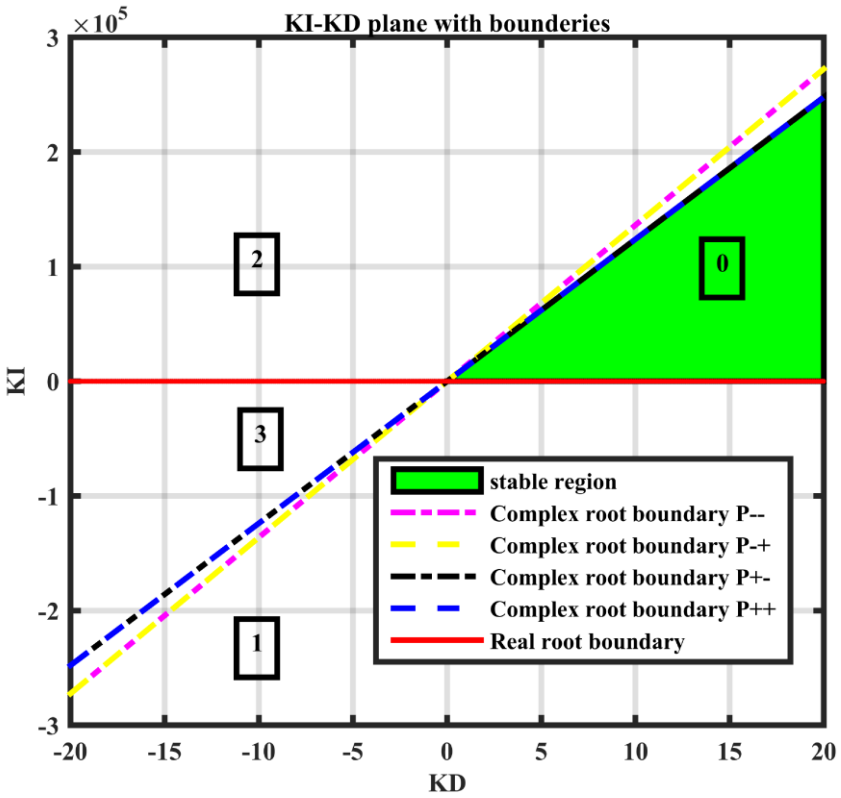

Figure 9: K_I and K_DPlane for P^{--},P^{-+},P^{+-} and P^{++}.

However, the edge polynomial in Table 2 as well as the vertex polynomial in Table 3 should be examined to guarantee robust stability in the case of the affine linear polynomial. Bialas theorem is used to establish a stable region for the KI and KD as mentioned in the previous section. For the edge polynomial $p^{(12)} = (1-\lambda)P^1(s) + \lambda P^2(s) \quad \lambda \in [0,1]$, $P^1(s) = P^{--}$ is one of the vertex polynomials in Table 3 it is stable from the previous section, $P^2(0) = K_I 4.5e7 > 0$ because $K_I > 0$, and the Hurwitz matrices of $(H_3^1)^{-1}H_3^2$ have three eigenvalues, one of them is equal to $1 > 0$ and the others are a function of K_I and K_D. However, we can chart the relationship as a line in the K_I and K_D plane to determine the ranges of the K_I and K_D which guarantees the robust stability of the closed-loop system as shown in Figure 13(a). The preceding approaches should be applied to the remaining edge polynomial families $p^{(13)}$, $p^{(42)}$, and $p^{(43)}$ where, Figure 13(b), Figure 13(c), and Figure 13(d) demonstrate regions of stability of the $p^{(13)}$, $p^{(42)}$ and $p^{(43)}$ respectively.

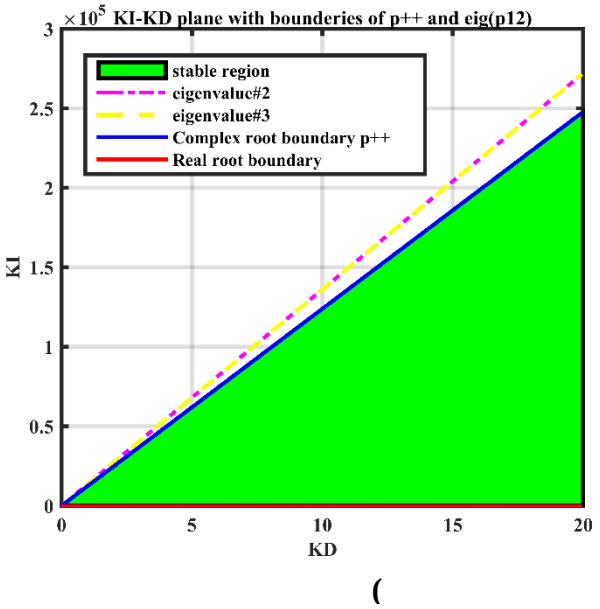

(

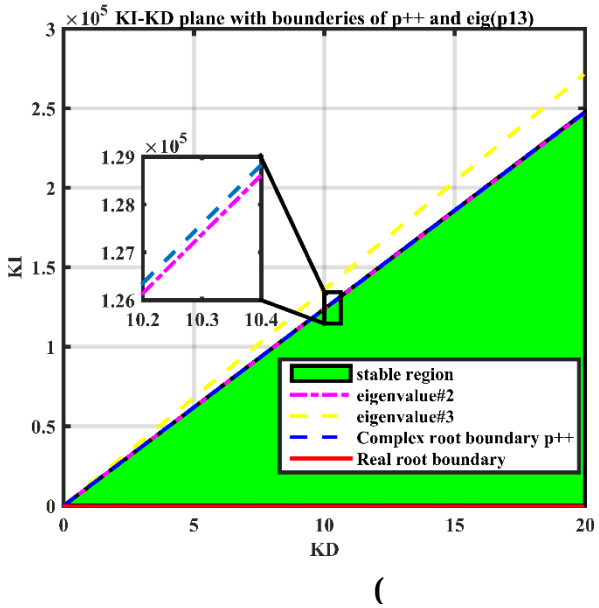

(

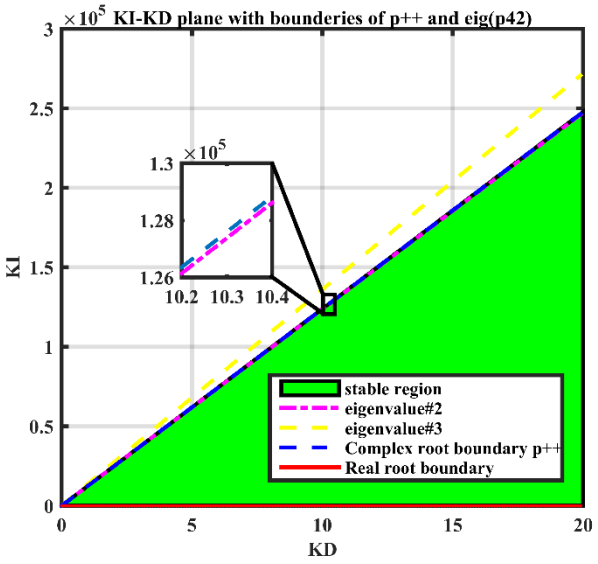

(

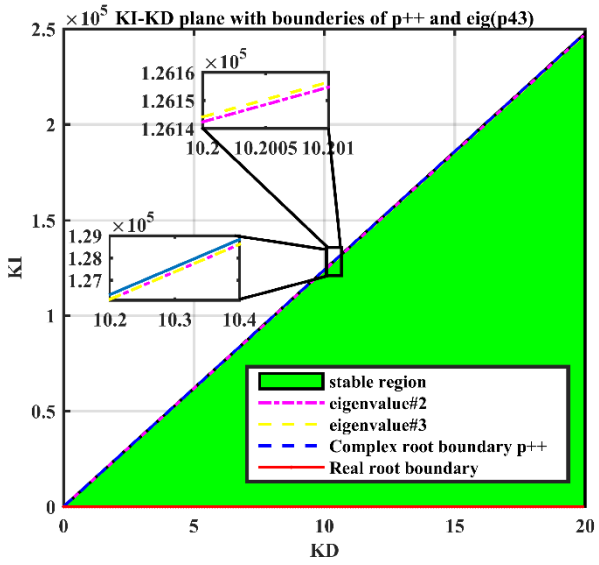

(

Figure 10: (a):K_I and K_D Plane for $P^{++}$and the eignvalues of P^{12}, (b):K_I and K_D Plane for $P^{++}$and the eignvalues of P^{13}, (c):K_I and K_D Plane for $P^{++}$and the eignvalues of P^{42},and (d):K_I and K_D Plane for $P^{++}$and the eignvalues of P^{43}

3.3 Artificial Bee Colony Algorithm for Optimization PID Controller

The Artificial Bee Colony (ABC) algorithm is a metaheuristic optimization method derived from nature and modeled after the feeding strategy of honeybees. Dervis Karaboga came up with the idea in 2005, and many other fields use it to address optimization issues. Honey bees naturally employ a collective intelligence strategy to locate the finest food sources[26-28]. The Artificial Bee Colony (ABC) optimization algorithm is a popular swarm intelligence technique inspired by the foraging behavior of honeybees. It is used to solve various optimization problems, including parameter tuning for control systems like PID (Proportional-Integral-Derivative) controllers. In control system engineering, PID controllers are widely used to regulate processes and systems. The PID controller uses three control gains: K_P (proportional gain), K_I (integral gain), and K_D (derivative gain) to adjust the control action based on the error signal, which is the difference between the desired setpoint and the actual process variable. The main goal of employing the ABC optimization algorithm for tuning the PID gains (K_P, K_I, and K_D) is to find the optimal combination of these gains that results in a well-performing and stable control system. The optimization process involves iteratively evaluating different sets of PID gains and updating them based on their performance. The ABC algorithm simulates the behavior of bees searching for the best food sources, and it does so by exploring the solution space to find the optimal PID gains.

Here's a general outline of how the ABC optimization algorithm can be employed for PID controller tuning:

1. **Initialization**: Generate an initial population of artificial bees, each representing a set of PID gains (K_P, K_I, and K_D), These gains are typically assigned random values within predefined bounds.
2. **Objective Function**: Define an objective function that quantifies the performance of the PID controller. This function measures how well the controlled system tracks the setpoint and how stable the system response is. In this research, the following function is used:

$$PFit = \frac{100}{2 * O.S + 6 * T_S + 12 * T_r} \tag{52}$$

Because of the fitness function is inversely proportional to a dynamical system's specific time domain step response requirements(small overshoot percentage with significant minimization of both settling and rising times), it should be altered for the maximum case.

1. **Employed Bees Phase:** In this phase, the fitness of each bee (solution) in the population is evaluated using the objective function. Bees then share information about their food sources (performance) with other bees within the hive. This phase can be stated mathematically as follows:

$$stepsize = rand_{(i)(j)} . (HB - HB[permute(i)(j)])$$
$$newHP = HB + stepsize \tag{49}$$

Where, HB is the Honey Bees, $rand_{(i)(j)}$ is an arbitrary number obtained based on the [-1,1] continuously normal distribution, $permute$ is several rows transposition functions, i represents the number of honey bees, and The number of dimensions of the problem is denoted by j.

1. **Onlooker Bees Phase:** Onlooker bees select food sources (solutions) probabilistically, with better-performing solutions having higher chances of being selected. The onlooker bees evaluate these selected solutions and share information further. The following expression can be used to determine a selection probability scheme:

$$P_i = PFit_i / \sum_{i=1}^{nHB} PFit_i \tag{50}$$

Where, nHB is the number of honey bees, and $PFit_i$ is the i^{th} food source's performance index function. A neighborhood source is established by adding a permutation-based random stepwise toward a randomly selected food source aside from herself when the i^{th} onlooker bee selects a food source (HB_{rws}) based on the roulette wheel selection scheme:

$$stepsize = rand_{(i)(j)} . (HB_{ros} - HB[permute(i)(j)])$$

$$newHP = \begin{cases} HB_{ros} + stepsize, & if\ rand < mr \\ HB_{ros}, & otherwise \end{cases} \quad (51)$$

Where; $0 \leq mr \leq 1$ is the modification rate.

2. **Scout Bees Phase:** Some bees become scout bees and are sent to explore new solutions randomly, beyond the existing solution space. This helps in diversifying the search and avoiding being trapped in local optima.
2. **Update Gains:** The best solution (food source) found during the process represents the optimal PID gains. These gains are then implemented in the control system.
3. **Termination:** The optimization process continues for a predefined number of iterations or until a stopping criterion is met.

Employed bees and Onlooker bees aim to improve their solutions depending on the knowledge available with each iteration of the ABC algorithm. The fitness of the solutions is assessed following each iteration, and the optimal solution is noted. Until a stopping requirement is satisfied, such as when the maximum number of iterations is reached or an optimal solution is attained, the process doesn't stop. The main steps of the ABC algorithm are demonstrated by the Flowchart of the ABC algorithm in Figure. 15. By employing the ABC optimization algorithm, researchers can effectively tune the PID gains (K_P, K_I, and K_D) for a specific control problem, leading to improved performance and stability in the controlled system. It is essential to carefully design the objective function and set appropriate bounds for the PID gains to ensure the algorithm's success in finding satisfactory solutions[29].

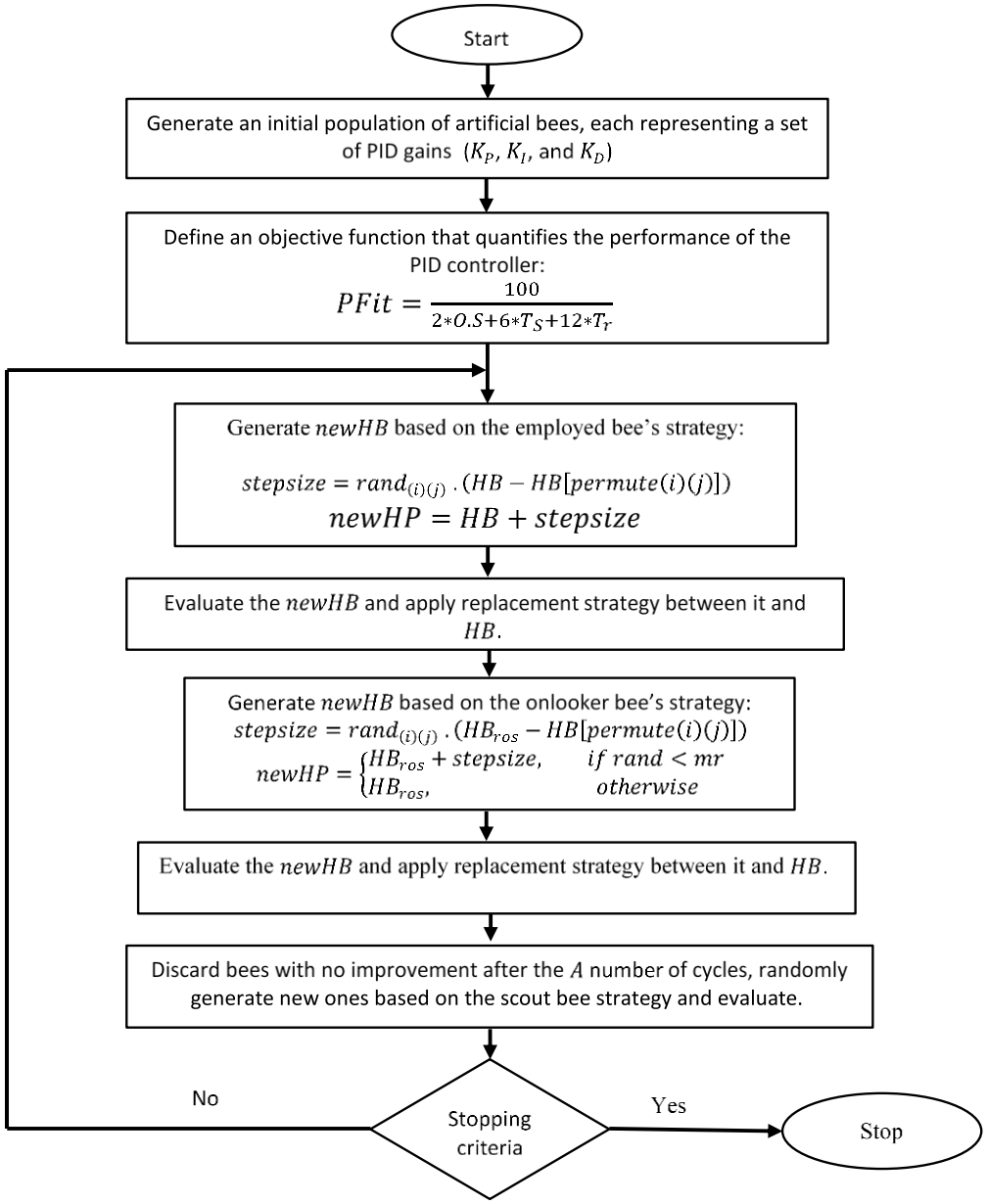

Figure 14: Flowchart of the ABC algorithm

4 RESULTS AND SIMULATION

For magnetic levitation, a linear Control scheme delivers good reaction, fast settling time, and high accuracy. However, the system's response is limited to a certain significant degree. The technique in practical systems will not be stable. Throughout the operation, the system will be exposed to considerable uncertainty. As a result, for such variations, traditional PID is ineffective. Some intelligent control strategies are considered to resolve this type of problem. The graphical parameter space methodology is one of the most effective methods in this circumstance. Which is demonstrated by this study.

The preceding section described the processes for locating all stabilization PID parameter locations for the CE152 Mglev system with parameter variations.

Table 4:

Response values for KP = 1, KI = 2000 and KD=5

Uncertain Parameters Values	$\boldsymbol{Tr(sec)}$	$\boldsymbol{Tp(sec)}$	**O.S %**	$\boldsymbol{Ts(sec)}$
$\boldsymbol{q_1 = 0.008, q_2 = 0.015}$	$2.0961e-05$	$4.9931e-05$	$\mathbf{26.6475}$	$1.2193e-04$
$\boldsymbol{q_1 = 0.0084, q_2 = 0.02}$	$2.1711e-05$	$5.1652e-05$	$\mathbf{25.6157}$	$1.2496e-04$
$\boldsymbol{q_1 = 0.0088, q_2 = 0.025}$	$2.2455e-05$	$5.1652e-05$	$\mathbf{24.6646}$	$1.2786e-04$

Table 4 shows how the performance differs in overshoot, rising time, settling time, and the peak time for the given system by choosing $KP = 1, KI = 2000, KD = 5$ as well as picking various values for uncertain parameters. Furthermore, Figure. 15 shows sample step responses with various locations within the specified ranges of parametric.

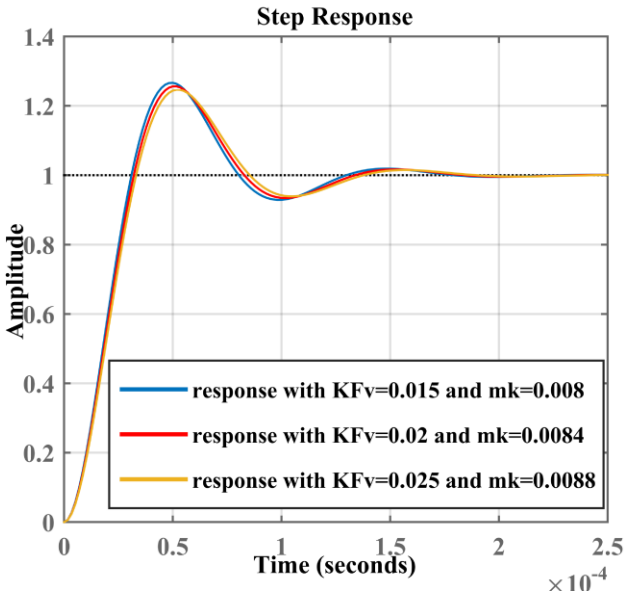

Figure 15: Step response of CE153 MAGLEV for different values of uncertain

The Artificial Bee Colony (ABC) optimization algorithm is used to elect an optimal of PID gains controllers [KP KD KI] within a stable region which maximizes the cost function. The search domains for [KP, KD, KI] are selected to be [10 0.5 10] for lower bounds and [15 1 100] for upper bounds. After 25 iterations in the (ABC) algorithm, the optimal matrix of PID gains controllers [KP KD KI] is obtained in Table 5. which highlights the disparities in overshoot, rising time, settling time, and peak time for the given system and selecting different values of uncertain parameters within the given regions $0.008 < q_1 = m_k = < 0.0088$ and $0.015 < q_2 = kFv < 0.025$. Moreover, Figure. 16 demonstrates the step response at the optimal of PID gains controllers [KP, KD, KI] and different points in the given ranges of the parametric uncertainties.

Table 5:
For the given system and picking alternative values of uncertain parameters, the performance varies in overshot, rising time, settling time, and peak time.

Uncertain Parameters values	**Optimal values of [KP KD KI]**	$PFit$	$Tr[sec]$	$Tp[sec]$	$O.S\,\%$	$Ts[sec]$
$q_1 = 0.008$, $q_2 = 0.015$	[10, 0.7798 , 10]	37462.5409	$1.1982 * 10^{-4}$	$3.2549 * 10^{-4}$	0	$2.0525 * 10^{-4}$
$q_1 = 0.0084$, $q_2 = 0.02$	[10.0014, 0.823 , 10]	37705.3697	$1.1909 * 10^{-4}$	$3.2548 * 10^{-4}$	0	$2.0384 * 10^{-4}$
$q_1 = 0.0088$, $q_2 = 0.025$	[10, 0.8865 , 10.7022]	39137.4098	$1.1509 * 10^{-4}$	$3.0825 * 10^{-4}$	0	$1.9566 * 10^{-4}$

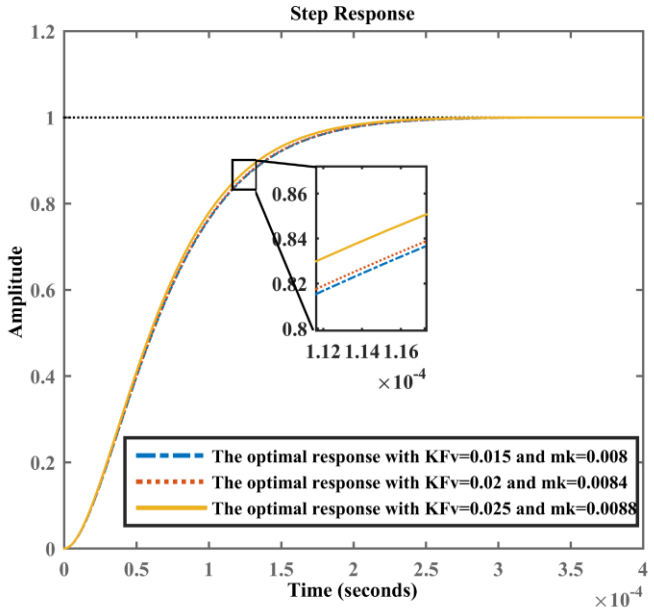

Figure 16: Step Response of Maglev for optimal values of PID gains

Figure. 17 depicts the iteration phase of the (ABC) algorithm. This displays how the value of the performance index increases for each iteration of the algorithm until it reaches its maximum value at the final stage.

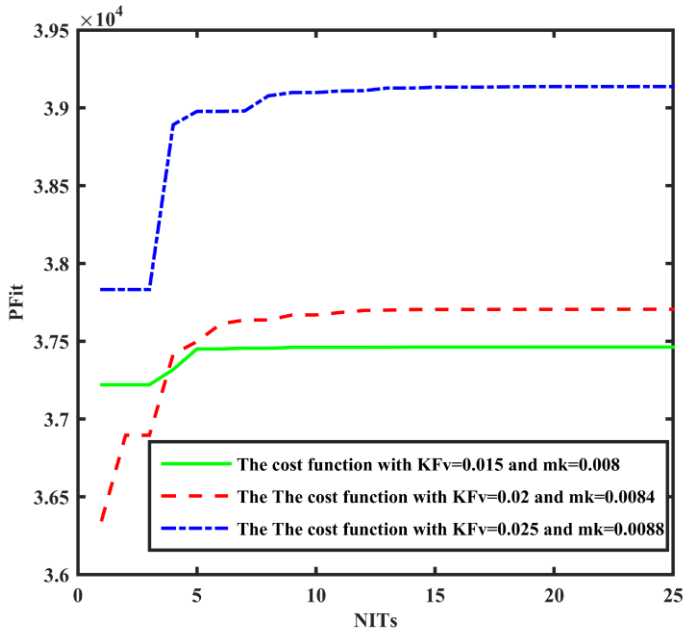

Figure 17: performance index value for each iteration (ABC) algorithm

5 CONCLUSION

Magnetic levitation systems offer a glimpse of the future of transportation with their potential for high-speed, energy-efficient, and comfortable travel. However, widespread adoption will depend on further advancements in technology, cost-effectiveness, and public acceptance. As research and development continue, magnetic levitation has the potential to revolutionize transportation and transform the way we move people and goods. In the scenario of uncertain parameters, all stabilized PID controller gains for the CE152 magnetic levitation system benchmark (Maglev) were studied and the results were in this study. A graphical parameter space method is implemented to identify all stabilized PID parameter regions. The (ABC) approach is used to find an optimal set of PID parameters [KP, KD, KI] that optimizes the objective functions within these stabilized PID parameter zones. The MATLAB simulation results prove that all stabilization PID parameter values can be chosen arbitrarily, resulting in a robustly stable CE152 magnetic levitation system with parameter variations in both. m_k and k_{Fv}.

REFERENCES

1. "Humusoft Praha,CE 512 Education Manual Magnetic Levitation Model," ed.
2. S. A. El Najjar, "Ripple Free Deadbeat Control for Nonlinear Systems with Time-Delays And Disturbances," 2013.
3. B. Hamed and H. Abu Elreesh, "Design of optimized fuzzy logic controller for magnetic levitation using genetic algorithms," *Journal of Information and Communication Technologies*, vol. 2, no. 1, 2012.
4. M. Ahmed, M. F. Hossen, M. E. Hoque, O. Farrok, and M. Mynuddin, "Design and construction of a magnetic levitation system using programmable logic controller," *American Journal of Mechanical Engineering*, vol. 4, no. 3, pp. 99-107, 2016.
5. H. Yaghoubi, "The most important maglev applications," *Journal of Engineering*, vol. 2013, 2013.
6. B.-Z. Kaplan and D. Regev, "Dynamic stabilization of tuned-circuit levitators," *IEEE Transactions on Magnetics*, vol. 12, no. 5, pp. 556-559, 1976.
7. J. R. Downer, "Analysis of a single axis magnetic suspension system," Massachusetts Institute of Technology, 1980.
8. N. J. Dahlen, "Magnetic active suspension and Isolation," Massachusetts Institute of Technology, Department of Mechanical Engineering, 1985.
9. M. Dussaux, "Status of the industrial applications of the active magnetic bearings technology," in *Turbo Expo: Power for Land, Sea, and Air*, 1990, vol. 79085: American Society of Mechanical Engineers, p. V005T14A016.
10. D. Limbert, H. Richardson, and D. Wormley, "Controlled dynamic characteristics of ferromagnetic vehicle suspensions providing simultaneous lift and guidance," 1979.
11. J. Paddison, C. Macleod, and R. Goodall, "State variable constraints on the performance of optimal Maglev suspension controllers," in *Control Applications, 1994., Proceedings of the Third IEEE Conference on*, 1994, pp. 599-604.
12. S. K. Pandey and V. Laxmi, "PID control of magnetic levitation system based on derivative filter," in *2014 Annual International Conference on Emerging Research Areas: Magnetics, Machines and Drives (AICERA/iCMMD)*, 2014: IEEE, pp. 1-5.
13. D. Maji, M. Biswas, A. Bhattacharya, G. Sarkar, T. K. Mondal, and I. Dey, "Maglev system modeling and lqr controller design in real time simulation," in *2016 International Conference on Wireless Communications, Signal Processing and Networking (WiSPNET)*, 2016: IEEE, pp. 1562-1567.
14. T.-E. Lee, J.-P. Su, and K.-W. Yu, "Implementation of the state feedback control scheme for a magnetic levitation system," in *2007 2nd IEEE Conference on Industrial Electronics and Applications*, 2007: IEEE, pp. 548-553.
15. M. Almobaied, H. S. Al-Nahhal, and K. B. Issa, "Computation Of Stabilizing PID Controllers For Magnetic Levitation System With Parametric Uncertainties," in *2021 International Conference on Electric Power Engineering–Palestine (ICEPE-P)*, 2021: IEEE, pp. 1-7.
16. I. Ahmad and M. A. Javaid, "Nonlinear model & controller design for magnetic levitation system," *Recent advances in signal processing, robotics and automation*, pp. 324-328, 2010.
17. N. Al-Muthairi and M. Zribi, "Sliding mode control of a magnetic levitation system," *Mathematical problems in engineering*, vol. 2004, no. 2, pp. 93-107, 2004.

18. X. Shi and Q. Mao, "Research on Control Strategy of Magnetic Levitation Gravity Compensator Based on Lyapunov Stability Criterion," in *IOP Conference Series: Materials Science and Engineering*, 2018, vol. 452, no. 4: IOP Publishing, p. 042146.
19. J. Ackermann, *Robust control: Systems with uncertain physical parameters*. Springer Science & Business Media, 2012.
20. D. Honc, "Modelling and identification of magnetic levitation model CE 152/revised," in *Computer Science On-line Conference*, 2018: Springer, pp. 35-43.
21. R. K. H. Galvão, T. Yoneyama, F. M. U. de Araújo, and R. G. Machado, "A simple technique for identifying a linearized model for a didactic magnetic levitation system," *IEEE Transactions on Education*, vol. 46, no. 1, pp. 22-25, 2003.
22. L. M. Belmonte, E. Segura, A. Fernández-Caballero, J. A. Somolinos, and R. Morales, "Generalised Proportional Integral Control for Magnetic Levitation Systems Using a Tangent Linearisation Approach," *Mathematics*, vol. 9, no. 12, p. 1424, 2021.
23. A. C. Bartlett, C. V. Hollot, and H. Lin, "Root locations of an entire polytope of polynomials: It suffices to check the edges," *Mathematics of Control, Signals and Systems*, vol. 1, no. 1, pp. 61-71, 1988.
24. M. Hypiusová, J. Osuský, and S. Kajan, "Robust Controller Design Using Edge Theorem for Modular Servo System," in *Technical Computing Prague 2007: 15th Annual Conference Proceedings*, 2007: Citeseer.
25. P. Dickinson and A. T. Shenton, "A parameter space approach to constrained variance PID controller design," *Automatica*, vol. 45, no. 3, pp. 830-835, 2009.
26. D. Karaboga, "An idea based on honey bee swarm for numerical optimization," Technical report-tr06, Erciyes university, engineering faculty, computer …, 2005.
27. D. Teodorovic and M. Dell'Orco, "Bee colony optimization–a cooperative learning approach to complex transportation problems," *Advanced OR and AI methods in transportation*, vol. 51, p. 60, 2005.
28. D. T. Pham, A. Ghanbarzadeh, E. Koç, S. Otri, S. Rahim, and M. Zaidi, "The bees algorithm—a novel tool for complex optimisation problems," in *Intelligent production machines and systems*: Elsevier, 2006, pp. 454-459.
29. A. Kaveh and T. Bakhshpoori, "Metaheuristics: outlines, MATLAB codes and examples," 2019.